SLAC-PUB-15090

Single- and Two-Photon-Induced Processes at the B Factories

Selina Z. Li

from the BaBar Collaboration
SLAC National Accelerator Laboratory
2575 Sand Hill Road MS61, Menlo Park, CA 94025, U.S.A

DOI: will be assigned

We discuss single- and two-photon-induced processes in e^+e^- annihilations with center-of-mass energy near 10.58 GeV from the BaBar and Belle experiments. In particular, we present experimental results from two-photon physics of $\gamma\gamma \to \pi^0\pi^0$ and $\gamma\gamma^* \to \pi^0$. We also review the observation of the Two-Virtual-Photon-Annihilation process ($e^+e^- \to \rho^0\rho^0$ and $e^+e^- \to \phi\rho^0$) and the observation of $e^+e^- \to \rho^+\rho^-$, which should be primarily a one virtual photon process, but whose angular distributions may imply potential interference effects.

1 Introduction

Single- and two-photon-induced processes can now be probed at high precision or low cross sections in e^+e^- collisions due to large integrated luminosity at the B factories. The majority of studies has been focused on single-photon-induced processes that produce final states with negative C-parity. The BaBar and Belle experiments are designed to study B physics from $\Upsilon(4S)$ production and its cross section is of the order of nanobarns. In contrast, the exclusive hadron pair production is low multiplicity and produced of the order of femtobarns. The hadron pair production over a wide range of effective center-of-mass (CM) energies via initial state radiation also emerged as an interesting avenue. They provide an excellent testing ground for QCD. On the other hand, two-photon-induced processes have final states with positive C-parity. Two-photon physics and Two-Virtual-Photon-Annihilation (TVPA) fall into this category. In fact the latter has only been first observed [1] in 2006.

In this proceeding, I will present experimental measurements for processes selected from those mentioned above. Results are based on data samples collected by the BaBar and Belle detectors, whose detailed descriptions can be found in Ref. [2] and [3], respectively. In particular, this proceeding will cover results obtained from two-photon physics and other one- or two-photon-induced e^+e^- processes, including $\gamma\gamma \to \pi^0\pi^0$, $\gamma\gamma^* \to \pi^0$, $e^+e^- \to \rho^0\rho^0$, $e^+e^- \to \phi\rho^0$, and $e^+e^- \to \rho^+\rho^-$.

Work supported in part by US Department of Energy contract DE-AC02-76SF00515.

2 Two-photon physics processes

Two-photon physics can be used to study resonance structures, i.e., look for new resonances produced by $\gamma\gamma$ interaction where only $C = +$ can be produced. This is a unique feature because $\gamma\gamma$ gives us extra access to states not produced directly in the beam particle annihilation. Also the $J = 0, 2$ angular momentum of $\gamma\gamma$ nicely complements the $J = 1$ annihilation. An example is the η_c. We can also use two-photon reactions to test the validity of various QCD models that predict the quark and gluon interaction and dynamics.

Two-photon physics can be studied using double-tag, single-tag, and no-tag. In a double-tag mode, the scattered e^+ and e^- are both detected and thus the full kinematic information is available. In a single-tag mode, only one scattered e^+ or e^- is detected while in the no-tag mode neither the e^+ or e^- is detected. There is increasing acceptance going from double-tag to no-tag, but decreasing kinematic information. The next two subsections will describe measurements using no-tag and single-tag analyses.

2.1 An analysis of $\gamma\gamma \to \pi^0\pi^0$

The virtual photon flux falls off rapidly at increasing two-photon CM energy W, so it had been difficult to use the two-photon reaction to study high-mass final states. The high luminosity of the B factories has now made this possible. In a no-tag analysis [4] with quasi-real photons, Belle analyzed a 223 fb^{-1} data sample to study the process $\gamma\gamma \to \pi^0\pi^0$. The production cross section as a function of W is measured from $0.6 - 4.1$ GeV. A partial wave analysis is performed to look at the angular dependence of the differential cross section for different energy bins. The data show a large-scattering-angle enhancement at low energy ($W < 1.9$ GeV) and begin to show a forward angle peak at high energy ($W > 2.0$ GeV). The fits to data in Figure 1 suggest that a G-wave becomes necessary and important at energy greater than 2 GeV.

In the higher energy region, a χ_{c0} charmonium state is observed with a significance of more than seven standard deviations, while χ_{c2} has a significance of about two standard deviations. The products of the two-photon decay width and the branching fraction for the two charmonium states with and without interference between χ_{c0} and continuum are shown in Table 1.

Interference	$\Gamma_{\gamma\gamma}(\chi_{c0})\mathcal{B}(\chi_{c0} \to \pi^0\pi^0)$ **(eV)**	$\Gamma_{\gamma\gamma}(\chi_{c2})\mathcal{B}(\chi_{c2} \to \pi^0\pi^0)$ **(eV)**
Without	$9.7 \pm 1.5 \pm 1.2$	$0.18^{+0.15}_{-0.14} \pm 0.08$
With	$9.9^{+5.8}_{-4.0} \pm 1.6$	$0.48 \pm 0.18 \pm 0.07 \pm 0.14$

Table 1: Products of the two-photon decay width and the branching fraction for the two charmonium states.

The right hand side of Figure 1 shows the W dependence of the cross section at high energy and in the angular region of $|\cos\theta^*| < 0.6$, where θ^* is the CM π^0 scattering angle. The cross section is fit to the power law $\sigma \sim W^{-n}$ for the region $3.1 < W < 4.1$ GeV exclusive of the charmonium region ($3.3 < W < 3.6$ GeV). The power $n = 6.9 \pm 0.6 \pm 0.7$ obtained from the fit for the $\pi^0\pi^0$ mode is compatible with $n = 7.9 \pm 0.4 \pm 1.5$ for the $\pi^+\pi^-$ mode [5]. The leading order pQCD prediction is $\sigma \sim W^{-6}$. The ratio of cross sections for neutral to charged pion-pair production is rapidly falling at low energies, but it is almost constant for $W > 3.1$ GeV. Table 2 compares this ratio with the leading term QCD [6], pQCD [7], and handbag model [8].

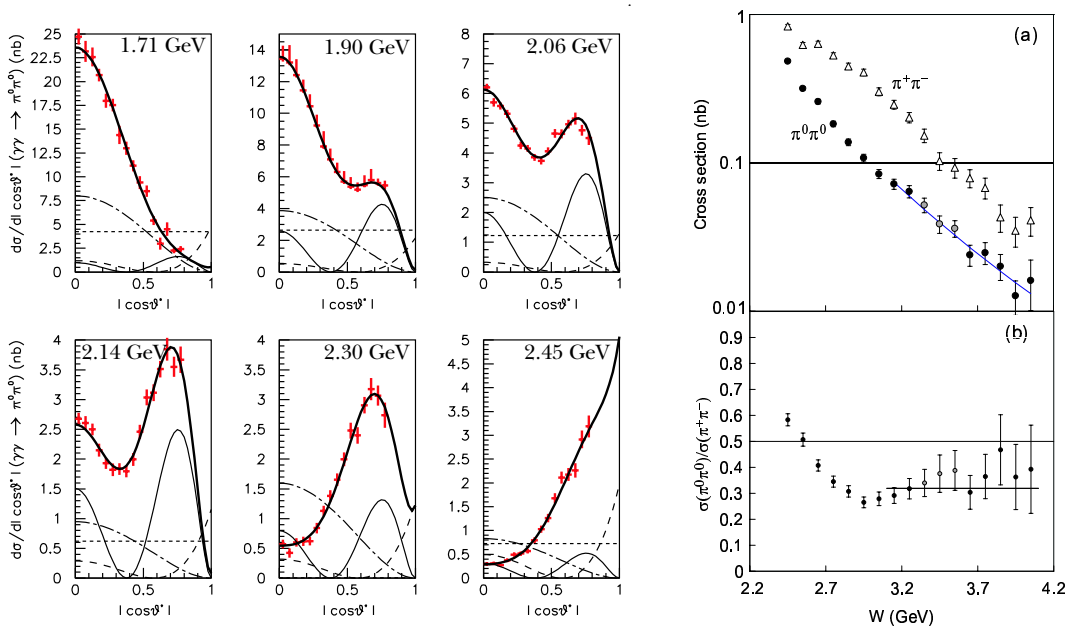

Figure 1: (Left) The angular dependence of the differential cross sections for $\gamma\gamma \to \pi^0\pi^0$ in six different W regions. (right) (a) The cross sections for $\gamma\gamma \to \pi^0\pi^0$ (circles) and $\gamma\gamma \to \pi^+\pi^-$ (triangles) as a function of W. (b) Ratio of the cross section for $\gamma\gamma \to \pi^0\pi^0$ to $\gamma\gamma \to \pi^+\pi^-$.

	Leading term QCD	**pQCD**	**Handbag model**	**Belle**
$\frac{\sigma(\pi^0\pi^0)}{\sigma(\pi^+\pi^-)}$	$0.03 - 0.07$	0.1	0.5	$0.32 \pm 0.03 \pm 0.05$

Table 2: Comparison of the ratio of neutral to charged pion-pair production cross sections.

2.2 A measurement of $\gamma\gamma^* \to \pi^0$ transition form factor

BaBar has made the measurement of $e^+e^- \to e^+e^-\gamma\gamma^*$, where $\gamma\gamma^* \to \pi^0$ in a single-tag analysis [9] based on 442 fb^{-1} of data. The π^0 in the final state is observed through its decay into two photons. The tagged electron must emit a highly virtual photon with a momentum transfer of $Q^2 > 3$ GeV^2 to be accepted by the detector. The momentum transfer to the untagged electron is close to zero. For the $\gamma\gamma^* \to \pi^0$ process, the differential cross section depends on only one form factor $F(Q^2)$. At high Q^2, the form factor can be represented as $F(Q^2) = \int T(x,Q^2)\phi_\pi(x,Q^2)\,\mathrm{d}x$, where x is the fraction of the π^0 momentum carried by one of the quarks, $T(x,Q^2)$ is the calculable hard scattering amplitude for $\gamma\gamma \to q\bar{q}$, and $\phi_\pi(x,Q^2)$ is the pion distribution amplitude for $q\bar{q} \to \pi$. Experimental measurement of the π^0 transition form factor $F(Q^2)$ helps determine the unknown dependence of $\phi_\pi(x,Q^2)$ on x.

To determine the number of events containing a π^0 in data, a binned likelihood fit to the $\gamma\gamma$ mass spectrum is performed in the π^0 region with a sum of signal and background distributions. This fitting procedure is applied in each of the 17 Q^2 intervals to study the Q^2 dependence of the cross section. The detector acceptance limits the detection efficiency at small Q^2. Therefore, to avoid possible systematics due to data-MC simulation differences near detector edges, we measure the cross section and form factor in the region $Q^2 > 4$ GeV^2.

In Figure 2 the measured differential cross section as a function of Q^2 at the Born level is compared to that from the CLEO experiment [10]. In the range $4 < Q^2 < 9$ GeV^2, BaBar results are in a reasonable agreement with CLEO data, but have significantly better precision. A $d\sigma/dQ^2 \sim Q^{-6}$ dependence in the range $12 < Q^2 < 30$ GeV^2 is observed in BaBar data. Also shown in Figure 2 is the π^0 transition form factor extracted from the cross section. At

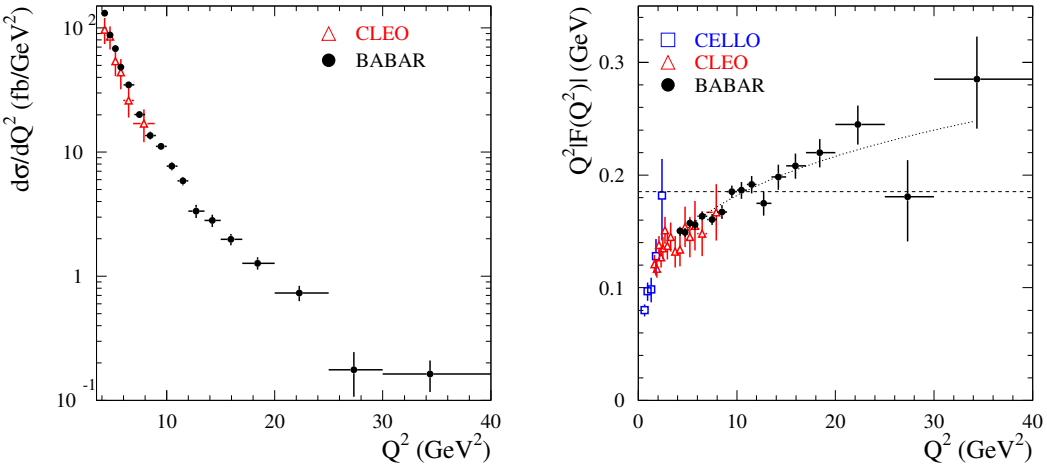

Figure 2: The $e^+e^- \to e^+e^-\pi^0$ differential cross section (left) and the $\gamma\gamma^* \to \pi^0$ transition form factor (right) as a function of Q^2. The dashed line shows the asymptotic limit for the form factor, and the dotted curve is a fit to BaBar data.

$Q^2 > 10$ GeV^2, the product $Q^2F(Q^2)$ exceeds the asymptotic limit of $\sqrt{2}f_\pi = 0.185$ GeV [11] and contradicts most existing theoretical models for the π^0 distribution amplitude [12]-[16]. A

fit to BaBar data in Figure 2 shows that $Q^2F(Q^2)$ is $\sim Q^{1/2}$ while the leading order pQCD predicts it to be constant in the asymptotic limit, thus suggesting that higher-order pQCD and power corrections are needed in the Q^2 region under study.

3 Selected processes from single-photon or two-photon

For a long time, we have understood that the process $e^+e^- \to$ hadrons at CM energy far below the Z mass is dominated by annihilation via a single virtual photon, thus yielding final states with $C = -1$. Very few studies are done for exclusive states with low multiplicity at 10 GeV due to the expectation of low rates, but there can be surprises. With the high luminosity collected at BaBar, TVPA in $e^+e^- \to \rho^0\rho^0$ and $e^+e^- \to \phi\rho^0$ [1] ($C = +1$) has been observed with production cross sections of a few femtobarns. This opens a new avenue for the study of hadron production mechanisms. In the next two subsections, selected results of exclusive hadron production from e^+e^- at 10.58 GeV at BaBar are presented.

3.1 $e^+e^- \to \rho^0\rho^0$ and $e^+e^- \to \phi\rho^0$

The first observation of $e^+e^- \to \rho^0\rho^0$ and $e^+e^- \to \phi\rho^0$ is based on 225 fb^{-1} of BaBar data from which events with exactly four well reconstructed, charged tracks with total charge zero are selected. Two oppositely charged tracks must be identified as pions and the other two as either pions or kaons. The invariant mass of the four charged tracks is required to be near the beam CM energy in order to be selected as $e^+e^- \to \pi^+\pi^-\pi^+\pi^-$ or $e^+e^- \to K^+K^-\pi^+\pi^-$ candidates. The scatter plots for $\pi^+\pi^-$ vs $\pi^+\pi^-$ or K^+K^- show strong signal peaks at the ρ^0 and ϕ mass. A binned log-likelihood fit over nine tiles is performed to extract signal in the $\rho^0\rho^0$ or $\phi\rho^0$ region. The extracted signal yields are 1243 ± 43 and 147 ± 13 for the $\rho^0\rho^0$ and $\phi\rho^0$ modes, respectively. The measured cross sections within the range $\cos\theta^* < 0.8$ are $20.7 \pm 0.7(\text{stat}) \pm 2.7(\text{syst})$ fb and $5.7 \pm 0.5(\text{stat}) \pm 0.8(\text{syst})$ fb for the $\rho^0\rho^0$ and $\phi\rho^0$ respectively, where θ^* is the production angle of ρ or ϕ in the CM frame. These results are consistent with calculations [17][18] from a vector-dominance two-photon exchange model provided after this measurement was released. As a comparison, $e^+e^- \to$ hadrons at 10 GeV is about 3 nb.

The $\rho^0\rho^0$ and $\phi\rho^0$ are final states with positive C-parity, so they cannot be produced via single-photon annihilation from e^+e^- collisions. However, they are allowed in TVPA as illustrated by the Feynman diagram in Figure 3. There are enough signal events to perform an angular analysis to investigate the production mechanism. The production angle θ^* shown in Figure 3 is forward peaking for these two processes, consistent with expectation of $\frac{\mathrm{d}\sigma}{\mathrm{d}\cos\theta^*} \propto \frac{1+\cos^2\theta^*}{1-\cos^2\theta^*}$ for TVPA. As a comparison, the $1 + \cos^2\theta^*$ distribution of single-photon annihilation is also shown. The helicity angles θ_H are also consistent with the $\sin^2\theta_H$ TVPA expectation for quasi-real photons.

3.2 Observation of $e^+e^- \to \rho^+\rho^-$

Given the observation of $e^+e^- \to \rho^0\rho^0$, it is natural to also look for the $\rho^+\rho^-$ final state with negative C-parity, which is expected to be produced dominantly via single-photon annihilation. BaBar has made the first observation of $e^+e^- \to \rho^+\rho^-$ [19] based on 379 fb^{-1} of data from which events with exactly two well reconstructed, oppositely charged tracks and two π^0 candidates are selected. The invariant mass of the four pions is required to be near the beam CM energy. The

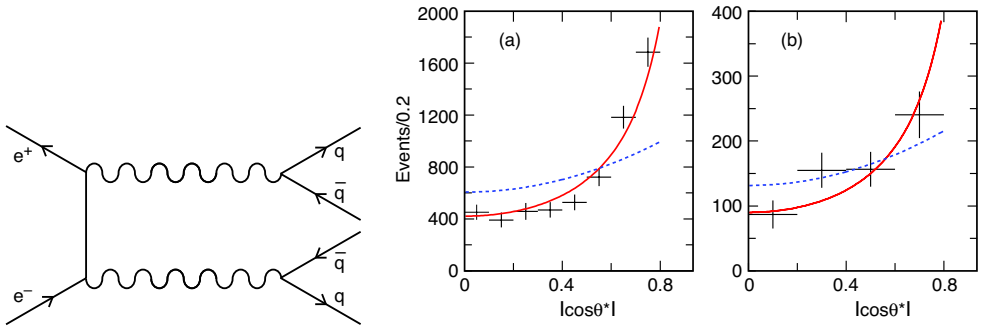

Figure 3: (Left) A Feynman diagram for the two-virtual-photon annihilation. (Right) The production angle distribution after correction for efficiency for (a) $e^+e^- \to \rho^0\rho^0$ and (b) $e^+e^- \to \phi\rho^0$. The solid and dashed curves are the normalized $\frac{1+\cos^2\theta^*}{1-\cos^2\theta^*}$ and $1+\cos^2\theta^*$, respectively.

$\pi\pi$ mass scatter plot shows strong peaks at the ρ mass. A 2D fit yields 357 ± 29 events with the cross section extrapolated to the full angular range measured to be $19.5 \pm 1.6(\text{stat}) \pm 3.2(\text{syst})$ fb. The large, clean sample of signal events allows us to perform an angular analysis to test QCD at the amplitude level.

Assuming a one-photon production mechanism, this vector-vector final state can be described by three independent helicity amplitudes, F_{00}, F_{10}, and F_{11}. The angular distributions for the helicity (azimuthal) angle $\theta_\pm$ ($\varphi_\pm$) of the pion from $\rho^\pm$ decay, and the ρ production angle θ^* are shown in Figure 4. Fits to the angular distributions with the normalization constraint $|F_{00}|^2 + 4|F_{10}|^2 + 2|F_{11}|^2 = 1$ reveal that $|F_{00}|^2 = 0.51 \pm 0.14(\text{stat}) \pm 0.07(\text{syst})$ which deviates from the perturbative QCD prediction of one (i.e., the F_{00} amplitude should dominate at high energy) by more than three standard deviations. This significant disagreement suggests that either the decay is not dominated by single-virtual-photon annihilation as expected, or the QCD prediction does not apply to data in this energy region. Because charged ρ's are involved, $\rho^+\rho^-$ cannot be produced via TVPA unless there is significant final state interaction. Given the possible relevance to potential similar effects in $B^0 \to \rho^+\rho^-$ process, which is crucial for the determination of angle α through CP-violation, understanding the observed $e^+e^- \to \rho^+\rho^-$ decay amplitudes may have broader implications.

4 Conclusion

Over the past nine years of operation, the B factories have integrated very high luminosity and have reopened several interesting areas for hadron physics. Belle provided a high statistics measurement of $\pi^0\pi^0$ production in two-photon physics and measured the cross section and its angular dependence in the kinematic range $0.6 < W < 4.1$ GeV and $|\cos\theta^*| < 0.8$ in a no-tag analysis. BaBar measured the $\gamma\gamma^* \to \pi^0$ transition form factor in a single-tag analysis and provided a gateway to study the pion distribution amplitude. Other single- and two-photon-induced e^+e^- processes are also reviewed. In particular, BaBar explored the cross sections and angular amplitudes of exclusive meson pair productions in e^+e^- annihilations. Studies of low multiplicity final states can provide an excellent testing ground for QCD. The case

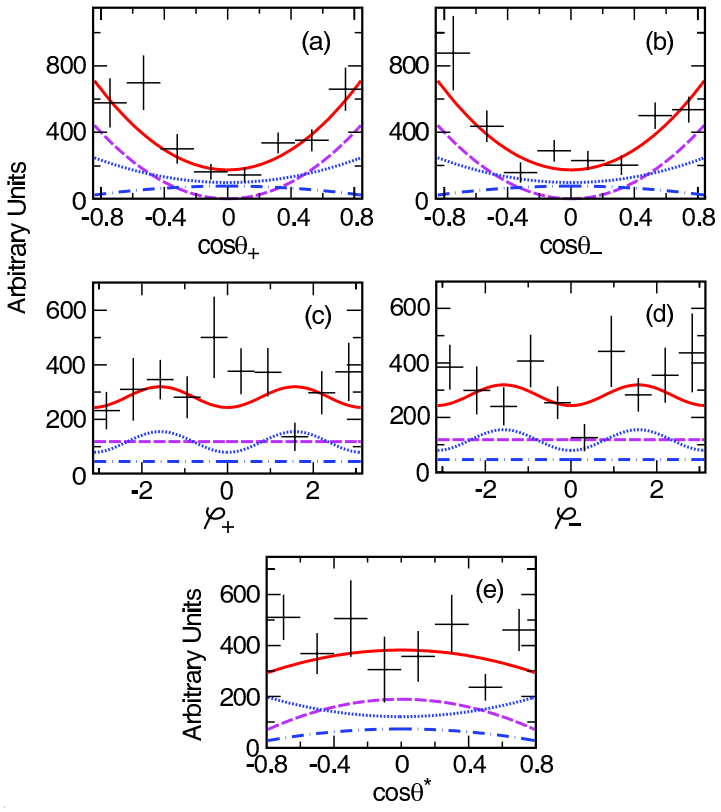

Figure 4: The angle distribution of (a) $\cos\theta_+$, (b) $\cos\theta_-$, (c) φ_+, (d) φ_-, (e) $\cos\theta^*$ after correction for efficiency for $e^+e^- \to \rho^+\rho^-$. See text for definition of the angles. The dashed curves show the contributions from F_{00}, the dotted curves are F_{10}, the dashed-dotted curves are F_{11}, and the solid curve is the total fit result.

of $e^+e^- \to \rho^+\rho^-$ is puzzling since it should be a one virtual photon process, but amplitude results suggest potential interference effects. Other possible final states should be explored to make use of the large datasets available at the B factories. In summary, nearly all of the measurements presented here show some deviations from models and thus are impetus to advance the theoretical front of our understanding.

References

[1] B. Aubert, *et al.*, Phys. Rev. Lett. **97**, 112002 (2006).

[2] B. Aubert, *et al.*, Nucl. Instrum. Methods **A479**, 1 (2002).

[3] A. Abashian, *et al.*, Nucl. Instrum. Methods **A479**, 117 (2002).

[4] S. Uehara, *et al.*, Phys. Rev. **D79**, 052009 (2009).

[5] H. Nakazawa, *et al.*, Phys. Lett. **B615**, 39 (2005).

[6] M. Benayoun and V.L. Chernyak, Nucl. Phys. **B329**, 285 (1990).

[7] S.J. Brodsky and G.P. Lepage, Phys. Rev. **D24**, 1808 (1981).

[8] M. Diehl, P. Kroll and C. Vogt, Phys. Lett. **B532**, 99 (2002).

[9] B. Aubert, *et al.*, arXiv:0905.4778, submitted to Phys. Rev. **D**.

[10] J. Gronberg, *et al.*, Phys. Rev. **D57**,33 (1998).

[11] G.P. Lepage and S.J. Brodsky, Phys. Rev. **D22**,2157 (1980).

[12] N.G. Stefanis, Nucl. Phys. Proc. Suppl. **181-182**, 199 (2008).

[13] A. Khodjamirian, Eur. Phys. J. **C6**, 477 (1999).

[14] V.L. Chernyak and A.R. Zhitnitsky, Nucl. Phys. **B201**, 492 (1982).

[15] G.P. Lepage and S.J. Brodsky, Phys. Lett. **B87**,359 (1979).

[16] A.P. Bakulev, S.V. Mikhailov, and N.G. Stefanis, Phys. Lett. **B508**,279 (2001).

[17] M. Davier, M. Peskin, and A. Snyder, hep-ph/0606155.

[18] G.T. Bodwin, *et al.*, Phys. Rev. **D74**, 074014 (2006).

[19] B. Aubert, *et al.*, Phys. Rev. **D78**, 071103 (2008).